A UNIFIED APPROACH FOR AUTOMATIC CAMERA CALIBRATION FROM VANISHING POINTS

Lazaros Grammatikopoulos [1], George Karras [1], Elli Petsa [2], Ilias Kalisperakis [1]

[1] Laboratory of Photogrammetry, Department of Surveying,
National Technical University of Athens (NTUA), GR-15780 Athens, Greece
[2] Laboratory of Photogrammetry, Department of Surveying,
Technological Educational Institute of Athens (TEI-A), GR-12210 Athens, Greece
E-mail: lazaros@central.ntua.gr, gkarras@central.ntua.gr, petsa@teiath.gr, ilias_k@central.ntua.gr

KEY WORDS: Automation, Calibration, Distortion, Edge, Extraction

ABSTRACT

A novel approach is presented for automatic camera calibration from single images with three finite vanishing points in mutually orthogonal directions (or of more independent images having two and/or three such vanishing points). Assuming 'natural camera', estimation of the three basic elements of interior orientation (camera constant, principal point location), along with the two coefficients of radial-symmetric lens distortion, is possible without any user interaction. First, image edges are extracted with sub-pixel accuracy, linked to segments and subjected to least-squares line-fitting. Next, these line segments are clustered into dominant space directions. In the vanishing point detection technique proposed here, the contribution of each image segment is calculated via a voting scheme, which involves the slope uncertainty of fitted lines to allow a unified treatment of long and short segments. After checking potential vanishing points against certain geometric criteria, the triplet having the highest score indicates the three dominant vanishing points. Coming to camera calibration, a main issue here is the simultaneous adjustment of image point observations for vanishing point estimation, radial distortion compensation and recovery of interior orientation in one single step. Thus, line-fitting from vanishing points along with estimation of lens distortion is combined with constraints relating vanishing points to camera parameters. Here, the principal point may be considered as the zero point of distortion and participate in both sets of equations as a common unknown. If a redundancy in vanishing points exists – e.g. when more independent images from the same camera with three, or even two, vanishing points are at hand and are to be combined for camera calibration – such a unified adjustment is undoubtedly advantageous. After the initial adjustment, the points of all segments are corrected for lens distortion to allow linking of collinear segments to longer entities, and the process is repeated. Data from automatic single-image calibrations are reported and evaluated against multi-image bundle adjustment with satisfactory results. Finally, further interesting topics of study are indicated.

1. INTRODUCTION

Camera calibration methods relying on the existence of vanishing points on single images have been presented in photogrammetry (Gracie, 1968; van den Heuvel, 1999; Bräuer-Burchardt & Voss, 2001; Grammatikopoulos et al., 2003) but also computer vision (Caprile & Torre, 1990; Liebowitz et al., 1999; Cipolla et al., 1999; Sturm & Maybank, 1999). Basically, this type of approach exploits parallelism and orthogonality among 3D lines commonly present in man-made environments. Indeed, the primary elements of interior orientation (camera constant and principal point) of single images can be estimated, together with the camera rotation matrix, from three orthogonal vanishing points (Merritt, 1958; Gracie, 1968). In this framework, results have also been reported using historic images (Karras & Petsa, 1999; Bräuer-Burchardt & Voss, 2001).

In computer vision, vanishing points in three orthogonal directions are often used for computing the image ω of the absolute conic, in order to subsequently decompose its expression for extracting the camera internal parameters as a 'calibration matrix' (Liebowitz et al., 1999; Sturm & Maybank, 1999); the same outcome is obtained by exploiting properties of the rotation matrix (Cipolla et al., 1999). In fact, as shown in Grammatikopoulos et al. (2004), such types of approach are essentially equivalent to the analytical photogrammetric scheme of Gracie (1968).

The authors have reported and assessed a formulation involving three vanishing points, in which the processes of line fitting, camera calibration (including radial lens distortion) and recovery of image attitude are all combined in one single step (Grammatikopoulos et al., 2003). However, imagery with pairs of vanishing points is much more common than that with three vanishing points suitable for camera calibration (e.g. none close to infinity). Without additional object constraints (see Bräuer-Burchardt & Voss, 2001), this kind of imagery can only supply the camera constant on the assumption of a fixed principal point (as used in Petsa et al., 1993, for rectifying historic images of demolished façades). Yet, a combination of more such images might supply equations sufficient for camera calibration purposes. Obviously, such images may well depict entirely different scenes as long as identical interior orientation is assumed.

Pursuing this thought, the authors recently developed a camera calibration algorithm which exploits the existence of vanishing points in two orthogonal directions on several independent, i.e. single, images (Grammatikopoulos et al., 2004). Using the relation of such pairs of vanishing points with the camera parameters, this algorithm relied on direct geometric reasoning regarding the locus of the projection centre in the image system. The centre of this hemispherical locus on the image plane lies halfway between the vanishing points, which also fix its diameter. This non-linear equation – which is independent of camera rotations – involves explicitly the interior orientation elements together with the image coordinates of the two vanishing points. Combination of such equations with line-fitting allowed simultaneous adjustment of all points on all lines of all views for estimating the three basic interior orientation elements, two coefficients of lens distortion and, optionally, image aspect ratio.

Here, this basic approach is extended to accommodate a single image with three vanishing points, but also sets of independent images with three and/or two vanishing points in orthogonal directions. Furthermore, the process runs now fully automatically,

by using an adaptation of the vanishing point detection method presented by Rother (2000).

Hence, camera calibration (with estimation of radial lens distortion) is carried out here iteratively in a unified least-squares adjustment of all points on imaged lines which concur in the three, or two, automatically detected vanishing points of the scene, on the hypothesis that these pertain to orthogonal directions in 3D space. Our algorithm thus differs from approaches in which parameter estimation is divided into two steps, with the calibration following an independent estimation of vanishing point location and lens distortion (van den Heuvel, 1999; Bräuer-Burchardt & Voss, 2001). In such instances, distortion refers to its point of 'best symmetry' (or simply to the image centre), and not to the image principal point $P(x_o, y_o)$ since the latter also participates as unknown in the next (calibration) step. Although it could also accommodate a distinct point of best symmetry, our unified algorithm accepts the principal point as the zero-point of distortion, which is the choice made in most practical situations.

However, more significant is the advantage of the simultaneous adjustment when there exists a redundancy in vanishing points, notably if more independent images – sharing the same camera geometry – with three and/or two vanishing points are at hand. In this case, the unified approach is advantageous (compared to two independent least-squares adjustment processes), since redundant vanishing points are constrained to reflect a unique camera geometry. Additionally, this approach might also be useful for images of a scene which are unsuitable for bundle adjustment (taken from standpoints close to each other, for instance).

2. CALIBRATION ALGORITHM

2.1 Line-fitting

In section 3 an automatic process for edge extraction, edge linking and detection of vanishing points is outlined. This results in groups of image line segments which converge to dominant vanishing points $V(x_V, y_V)$. If x, y are the observed image coordinates of an individual point on such a line segment, introduction of coefficients k_1, k_2 of radial symmetric lens distortion into the parametric equation of a 2D line gives:

$$\left[x - \left(x - x_o \right)\left(k_1 r^2 + k_2 r^4 \right) - x_V \right]\cos\theta +$$
$$+ \left[y - \left(y - y_o \right)\left(k_1 r^2 + k_2 r^4 \right) - y_V \right]\sin\theta = 0 \quad (1)$$

with r denoting the radial distance of this particular image point from the principal point (x_o, y_o). Eq. (1) represents the observation equation for the common adjustment of all line segments. It relates the observed quantities x, y (whose sum of squared residuals is to be minimised), the coordinates of the corresponding vanishing point, the principal point coordinates and the coefficients of radial lens distortion.

2.2 The 'calibration sphere'

Concerning camera calibration itself, Grammatikopoulos et al. (2004) have pointed to the fact that every pair V_1, V_2 of vanishing points of orthogonal directions constraints the image projection centre O on a geometric locus, from whose points the segment $V_1 V_2$ is seen under a right angle. This hemisphere ('calibration sphere') has the midpoint of segment $V_1 V_2$ as its centre and the distance $V_1 V_2$ as its diameter. All points on this surface represent a possible projection centre, whose distance from the image plane provides a corresponding camera constant c, while

its projection onto it fixes the principal point P (for a more detailed geometric reasoning see Grammatikopoulos et al., 2004).

The analytical equation of this sphere can be written as:

$$\left(x_o - x_m \right)^2 + \left(y_o - y_m \right)^2 + c^2 = R^2 \quad (2)$$

with
$$x_m = \frac{x_1 + x_2}{2} \qquad y_m = \frac{y_1 + y_2}{2}$$

and
$$R = \frac{\sqrt{\left(x_1 - x_2 \right)^2 + \left(y_1 - y_2 \right)^2}}{2}$$

whereby c is the camera constant, (x_o, y_o) is the principal point, (x_1, y_1), (x_2, y_2) are the two vanishing points, while (x_m, y_m) is the centre of the sphere and R its radius. Three pairs of vanishing points of orthogonal directions fix three such spheres; their intersection fixes the projection centre in image space (Fig. 1).
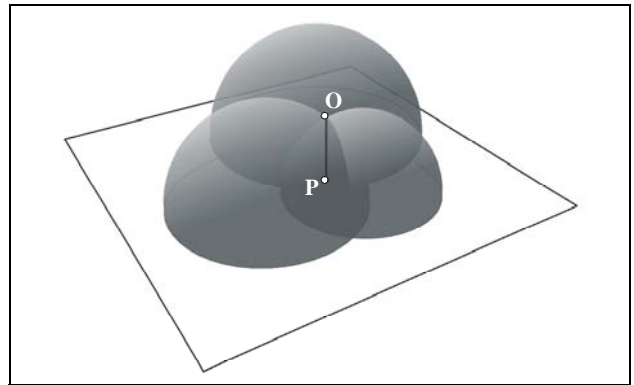

Figure 1. Projection centre O as intersection of three calibration spheres and principal point P as its projection on the image.

This minimum of three pairs of vanishing points may be drawn either from a single image with three vanishing points or, equivalently, from three separate images each having two vanishing points (in the second case it is assumed that these three separate images do not produce spheres which are close to coincidence). While three such vanishing points allow estimating only the primary internal camera elements (c, x_o, y_o), other parameters such as the image aspect ratio may be estimated if an additional pair of vanishing points is known (Grammatikopoulos et al., 2004). Clearly, any additional pair of vanishing points beyond the minimal requirement gives rise to a redundant 'calibration sphere'.

2.3 The calibration adjustment

The calibration adjustment involves the observation equations – one Eq. (1) for each point of all line segments passing through a vanishing point – and the constraint equations Eq. (2); the latter introduce the camera constant as an additional unknown. Shared unknowns are the coordinates of all vanishing points and those of the principal point. In our experience, if Eqs. (2) are treated as observation equations with very large weights rather than as strict constraints, it appears that in many cases initial values for distortion coefficients k_1, k_2 may be simply set to zero.

3. DETECTION OF VANISHING POINTS

As mentioned already, the camera calibration phase is preceded here by the automatic extraction, linking and grouping of image edges which concur to vanishing points. A large literature exists on automatic detection of vanishing points, after Barnard (1983) first introduced the use of the Gaussian Sphere as an accumula-

tion space (e.g. Magee & Aggarwal, 1984; Quan & Mohr, 1989; Gallagher, 2002). A comparison of parameterisation models of the Gaussian Sphere with respect to noise is found in Wenzel & Grigat (2006). Other approaches include, for instance, those of Straforini et al. (1993), Shufelt (1999), Antone & Teller (2000), Rasmussen (2004). The procedure adopted here, which relies on Rother (2000), comprises the steps of edge extraction and linking and that of vanishing point detection.

3.1 Edge extraction and linking

Initially image edges are extracted with sub-pixel precision and then linked to line segments through polygonal approximation. A suitable threshold for edge 'straightness' (Thormaehlen et al., 2003) regulates the tolerated distance of edge points from a line segment. Line parameters are estimated with least-squares line-fitting, while very short segments are discarded. The size of the latter threshold is reduced after the first estimation of the radial lens distortion polynomial (see Section 3.3).

Next, extracted line segments are to be clustered in groups corresponding to dominant space directions. The orthogonality criterion of space line directions is used for establishing vanishing points of three mutually orthogonal directions (van den Heuvel, 1998; Rother, 2000).

3.2 Vanishing point detection

The intersections of all possible pairs of line segments represent potential vanishing points. Rother (2000) allows every segment s to vote for each such point with the sum of two weighted contributions (a voting scheme also adopted in Bauer et al., 2002). The first refers to the angle α (if it falls below a threshold α_0) between s and the line joining its midpoint M with the potential vanishing point. The other weighted component is proportional to segment length. The added votes from all accepted segments produce the final strength of a potential vanishing point. Rother (2002) gives empirical values for the two weighting factors.

Here, a uniform treatment of long and short segments dispenses with weighting factors. The covariance matrix of the initial line-fitting adjustment gives an estimate for the standard error σ_θ of the slope angle of each line. However, this can also be regarded as the uncertainty of α (Fig. 2). Thus, $\alpha + \sigma_\theta$ is a realistic estimation of angle α formed by segment s and line VM.
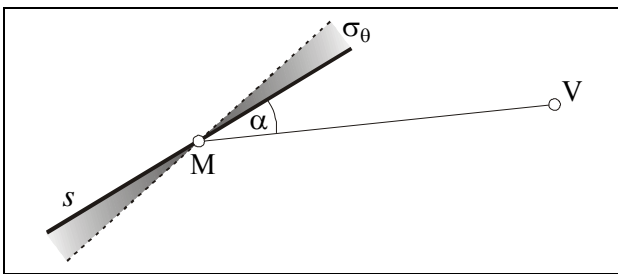

Figure 2. Angle α (formed by segment s and the line joining its midpoint M with potential vanishing point V) and error σ_θ.

The standard error σ_θ reflects the effect of noise as well as that of the geometry of the line-fitting adjustment, in which segment length plays a central role. In this sense, vote v of each segment for a particular vanishing point may be simply computed as

$$v = 1 - \frac{\alpha + \sigma_\theta}{\alpha_0} \qquad (3)$$

whereby α_0 is a threshold value. Votes from all segments with $(\alpha + \sigma) < \alpha_0$ for some potential vanishing point are summed to

produce the total score for this particular candidate. The contribution of the error of segment midpoint M to the uncertainty of α is regarded as negligible compared to that of line slope.

Potential vanishing points along with their final scores are next checked, after Rother (2000), against geometric criteria for determining three dominant vanishing points of orthogonal space directions. If one vanishing point is at infinity, only the locus of the principal point may be found (segment of the vanishing line defined by the other two points); if only one vanishing point is finite, it represents the principal point (yet the camera constant remains undetermined). Since our primary concern here is a full camera calibration, only triplets of finite vanishing points which form acute triangles are considered in the search process (orthogonality criterion). Besides, a principal point (orthocentre of the triangle defined by the vanishing points) is expected to be close to the image centre. Finally, computed camera constants should have 'reasonable' values (camera criterion). All vanishing point triads which meet these criteria are accepted and sorted according to total score; that with the highest score is selected as the final triad of dominant vanishing points.

3.3 Edge linking after correction of lens distortion

Obviously, the extracted edges and subsequent edge linking are affected by radial lens distortion. To reduce this effect, the co-efficients of radial lens distortion estimated in the first iteration of the calibration adjustment are used for correcting the initially extracted edge points. Next, with a lower threshold on 'straight-ness', edge linking is repeated to produce longer line segments. The search among the new potential vanishing points results in a final triplet. Their position is optimized in a least-squares adjustment to refine the values for line slopes. In order to identify in a group of convergent line segments those actually belonging to the same line, all segments are checked in pairs. If the overall RMS distance of all points of both segments from the fitted line equation of the other segment does not exceed a threshold, such line segments are seen as parts of the same image line and are treated as such in the next iteration.

4. PRACTICAL EVALUATION

The six 800×600 images of Fig. 3 were used in an experimental evaluation of the approach. The camera has a moderate field of view (~ 60°), while all vanishing points of the vertical space direction are indeed far from the image centre. This allows testing the method under realistic conditions. Examples for line extraction and clustering are seen in Fig. 4 (for the last image of Fig. 3). On the left, initial extracted edges above the length threshold of 20 pixels are shown. Among them, those edges converging to the three dominant vanishing points were singled out by means of an angular threshold $\alpha_0 = 2°$ (centre). The final segments, generated after correction of radial lens distortion and used for the final calibration, are presented on the right. Two segments were treated as parts of the same line if the overall RMS distance of their points from the line equation of the other segment did not exceed 2 pixels. Calibration results from single images as well as from their common adjustment are shown in Table 1, where σ_o represents the standard error of adjustments (the rather large values of σ_o are due to the threshold for segment linking).

However, it is generally difficult to quantify the performance of calibration approaches exclusively with real images, due to lack of ground truth (Swaminathan & Nayar, 2000). The consistency of results from different images is a significant indication for repeatability, though not for 'closeness to truth'. Available calibration data from other methods may also be used for checking, yet it is noted that parameter values may be tied to each other

by strong correlations. Probably, direct comparisons in terms of 3D model reconstruction is a more conclusive criterion. With this in mind, the nine images of Fig. 5 (among them four of those taking part in single-image calibration) were used in a self-calibrating bundle adjustment without external control, based on 30 tie points. Results are also seen in Table 1.
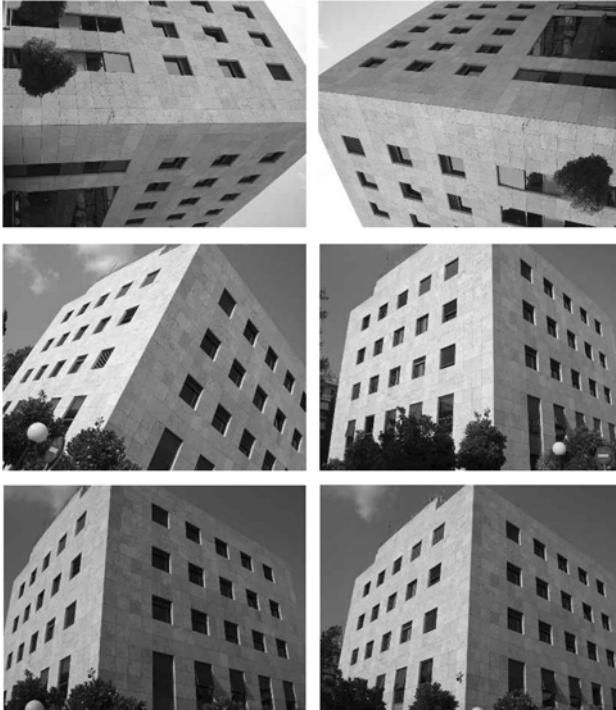

Figure 3. Images used for calibration from vanishing points.

Figure 4. Initial edges (above), segments grouped in vanishing points (middle), segments after correction of distortion (below).

Table 1. Calibration results						
images	c (pixel)	x_o (pixel)	y_o (pixel)	k_1 ($\times10^{-8}$)	k_2 ($\times10^{-13}$)	σ_o (pixel)
1 *124 lines*	896.17 ± 0.80	6.81 ± 0.63	–15.35 ± 0.88	–8.65 ± 0.59	–1.64 ± 0.25	0.45
2 *134 lines*	897.31 ± 0.81	11.41 ± 0.70	–10.92 ± 1.09	–9.03 ± 0.63	–2.38 ± 0.26	0.44
3 *88 lines*	908.17 ± 1.66	14.17 ± 2.12	–6.81 ± 1.45	–11.67 ± 0.97	–1.39 ± 0.42	0.40
4 *94 lines*	900.20 ± 1.23	13.93 ± 1.62	–8.29 ± 0.75	–4.30 ± 0.83	–3.97 ± 0.33	0.39
5 *84 lines*	902.52 ± 1.40	3.48 ± 1.79	–5.54 ± 1.14	–7.67 ± 0.80	–2.68 ± 0.29	0.36
6 *88 lines*	903.60 ± 1.28	18.49 ± 1.89	–2.57 ± 0.83	–7.47 ± 0.70	–3.41 ± 0.26	0.39
all *612 lines*	899.21 ± 0.39	10.67 ± 0.35	–8.99 ± 0.33	–7.82 ± 0.29	–2.56 ± 0.12	0.42
bundle adjustment	905.63 ± 3.15	9.22 ± 1.42	–6.00 ± 1.60	–8.31 ± 1.07	–2.79 ± 0.49	0.26

Calibration data from vanishing points of single images appear as coherent. Individual values for the camera constant c deviate by less than 1% from their mean value and from that of the solution with all images. Further, all c-values are within the range $c \pm 3\sigma_c$ of bundle adjustment. In fact the values for c which correspond to the calibrated distortion curves (see Fig. 6 below) are somewhat more coherent. In general, differences of few pixels in principal point location should be expected (as it often occurs also in different bundle adjustments). It is notable that (given that the vanishing point of the vertical space direction is indeed 'weak') the first two images in Fig. 3, acquired with a 90° rotation, gave for x_o the closest values to that of bundle adjustment, whereas these same images display the largest differences in y_o – a fact pointing to the importance of geometry.
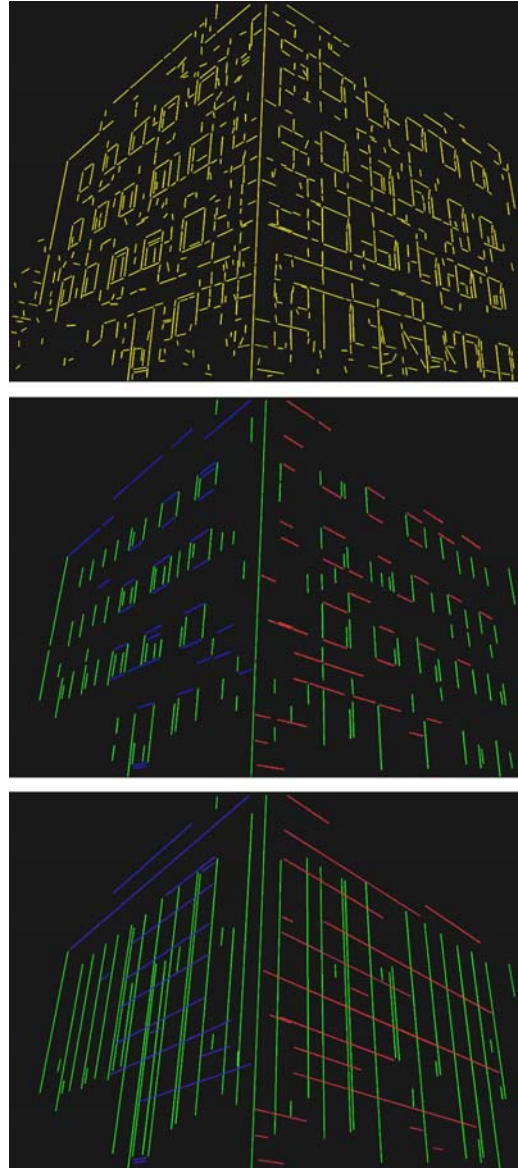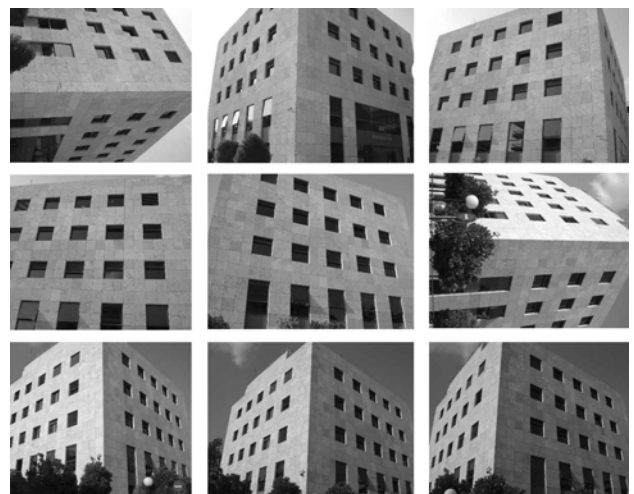

Figure 5. Images used in self-calibrating bundle adjustment

Calibration from vanishing points leads here to almost identical curves of radial distortion, which also practically coincide with

that from bundle adjustment. Fig. 6 shows the calibrated curves of radial lens distortion Dr.
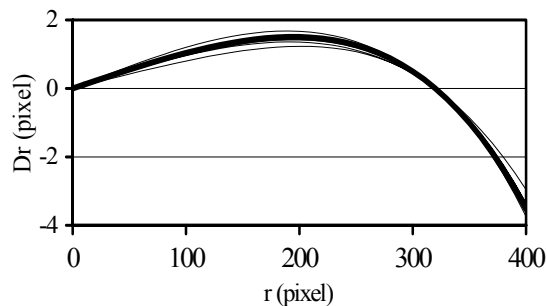

Figure 6. Calibrated distortion curves from vanishing points and from bundle adjustment (dark line).

The actual impact of differences between the calibration results is probably best assessed in terms 3D reconstruction, since discrepancies may solely be attributed to different calibration data. Thus, model coordinates of all tie points were determined in true scale with bundle adjustments using calibration results from vanishing points as fixed. They were then compared with tie point coordinates from the self-calibrating solution. Standard errors σ of the 3D similarity transformation between object points reconstructed with pre-calibration using vanishing points and self-calibration are seen in Table 2. The values have also been reduced to the mean pixel size in object space.

Table 2. Accuracy of 3D reconstruction		
calibration data	σ (cm)	σ (pixel)
from image 1	2.1	1.2
from image 2	2.0	1.1
from image 3	0.9	0.5
from image 4	0.8	0.5
from image 5	1.0	0.6
from image 6	1.2	0.7
from all images	1.1	0.7

The above results indicate that calibration values obtained automatically from individual images with no external control have allowed satisfactory 3D reconstruction in the case of an object with significant extension in depth. In fact, taking into consideration that the data which served as 'ground truth' (from a self-calibrating bundle adjustment) are also subject to uncertainty, one may assert that here the precision of reconstruction is about 1 pixel in object space.

5. CONCLUSION

An automatic camera calibration approach, which is based on at least three pairs of vanishing points of orthogonal space directions (on one, or more, images from the same camera) has been developed, implemented and tested. A main feature here is that camera constant, principal point location, two coefficients of radial-symmetric lens distortion as well as image vanishing points are all estimated iteratively in a unified least-squares adjustment of all image points belonging to lines which converge in the dominant vanishing points. Furthermore, this algorithm may well accommodate independent imagery of totally different scenes. The approach is intended exclusively for camera calibration, i.e. it does not involve image rotation matrices. Line segments are extracted and associated with a particular vanishing point in a fully automatic mode, based on a modification of the method of Rother (2000); edges are re-linked after correction for lens distortion as estimated in the first iteration.

Obviously, evidence from further experiments is needed. However, the evaluation against self-calibrating multi-image bundle adjustment (with no external control) has indicated that results from the automatic calibration approach with vanishing points reported here may, in principle, provide information on camera geometry which is definitely suitable for initialisation purposes, but apparently also as pre-calibrated camera parameter values in tasks of 'moderate' accuracy requirements.

Of course, further questions also need to be addressed. These include the introduction of robust estimators into the adjustment (Aguilera et al., 2005), the issue of vanishing points tending to infinity, an investigation regarding the effect of noise as well as an extension of the geometric model for full camera calibration including image skewness. Nevertheless, one has to admit that such calibration approaches – which rest on a mere assumption of mutually orthogonal space directions – are inherently subject to notable limitations and seek to reconcile rather contradictory aspects. For instance, their accuracy depends, among others, on the distribution of extracted line segments over an image frame, but at the same time also on an 'adequate' perspective distortion of the imaged scene (or, put more generally, on the shape of the triangle defined by three vanishing points of orthogonal space directions). Such questions, too, outline an interesting field for further study.

REFERENCES

Aguilera, D.G., Gómez Lahoz, J., Finat Codes, J., 2005. A new method for vanishing points detection in 3D reconstruction from a single view. Int. Workshop on 3D Virtual Reconstruction and Visualization of Complex Architecture (3D-ARCH '05), Venice.

Antone, M. Teller, S., 2000. Automatic recovery of relative camera rotations for urban scenes. IEEE Conf. on Computer Vision & Pattern Recognition, vol. 2, pp. 282-289.

Barnard, S.T. 1983. Interpreting perspective images. Artificial Intelligence, 21, pp. 435-462.

Bauer, J., Klaus, A., Karner, K., Zach, C., Schindler, K., 2002. MetropoGIS: a feature based city modeling system. Proc. Photogrammetric Computer Vision, ISPRS Comission III Symposium, Graz, Austria (in CD).

Bräuer–Burchardt, C., Voss, K., 2001. Image rectification for reconstruction of destroyed buildings using single views. In: B. Fisher, K. Dawson-Howe, C. O'Sullivan (eds.), Virtual & Augmented Architecture, Springer, pp. 159-170.

Caprile, B., Torre, V., 1990. Using vanishing points for camera calibration. Int. Journal of Computer Vision, 4(2), pp. 127-140.

Cipolla, R., Drummond, T., Robertson, D.P., 1999. Camera calibration from vanishing points in images of architectural scenes. Proc. 10th British Machine Vision Conference, pp. 382-391.

Gallagher A.C., 2002. A ground truth based vanishing point detection algorithm. Pattern Recognition, 35(7), pp. 1527-1543.

Gracie, G., 1968. Analytical photogrammetry applied to single terrestrial photograph mensuration. XI ISP Congress, Lausanne.

Grammatikopoulos, L., Karras, G., Petsa, E., 2003. Camera calibration approaches using single images of man-made objects. Proc. 19th CIPA Int. Symposium, Antalya, pp. 328-332.

Grammatikopoulos, L., Karras, G., Petsa, E., 2004. Camera calibration combining images with two vanishing points. Int. Arch.

of Photogrammetry, Remote Sensing and Spatial Information Sciences, 35 (Part 5), pp. 99-104.

Karras G., Petsa E., 1999. Metric information from single uncalibrated images. Proc. 17th CIPA Int. Symp., Olinda (in CD).

Liebowitz, D., Criminisi, A., Zisserman A., 1999. Creating architectural models from images. Eurographics '99, Computer Graphics Forum, 18(3), pp. 39-50.

Magee M., Aggarwal J., 1984. Determining vanishing points from perspective images. Computer Vision, Graphics and Image Processing, 26, pp. 256–267.

Merritt, E.L., 1958. Analytical Photogrammetry. Pitman Publ. Co., New York.

Petsa, E., Karras, G., Aperghis, G., 1993. Zur Fassadenentzerrung aus Amateurbildern niedergerissener Altstadtviertel. Zeitschrift f. Vermessungswesen u. Raumordnung, 58(8):431-436.

Quan, L., Mohr, R., 1989. Determining perspective structures using hierarchical Hough transform. Pattern Recognition Letters, 9, pp. 279-286.

Rasmussen, C., 2004. Texture-based vanishing point voting for road shape estimation. Proc. British Machine Vision Conference, 7-9 September, London, UK.

Rother C., 2000. A new approach for vanishing point detection in architectural environments. Proc. 11th British Machine Vision Conference, pp. 382–391.

Rother, C., 2002. A new approach to vanishing point detection in architectural environments. Image and Vision Computing, 20(9-10), pp. 647-655.

Shufelt, J.A.,1999. Performance evaluation and analysis of vanishing point detection techniques. IEEE Trans. Pattern Analysis and Machine Intelligence, 21(3), pp. 282–288.

Straforini, M., Coelho, C., Campani M., 1993. Extraction of vanishing points from images of indoor and outdoor scenes. Image and Vision Computing, 11(2), pp. 91-99.

Sturm, P., Maybank, S. J., 1999. A method for interactive 3D reconstruction of piecewise planar objects from single images. Proc. 10th British Machine Vision Conference, pp. 265-274.

Swaminathan R., Nayar, S., 2000. Non-metric calibration of wide-angle lenses and polycameras. IEEE Trans. Pattern Analysis and Machine Intelligence, 22(10), pp. 1172-1178.

Thormaehlen, T., Broszio, H., Wassermann, I., 2003. Robust line-based calibration of lens distortion from a single view. Proc. Mirage 2003, Rocquencourt, France, pp. 105-112.

van den Heuvel, F., 1999. Estimation of interior orientation parameters from constraints on line measurements in a single image. Int. Arch. Photogrammetry & Remote Sensing, 32 (5W11), pp. 81-88.

van den Heuvel F., 1998. Vanishing point detection for architectural photogrammetry. Int. Arch. Photogrammetry and Remote Sensing, 32(B5), pp. 652-659.

Wenzel, F., Grigat, R., 2006. Representing directions for Hough Transforms. Proc. Int. Conference on Computer Vision Theory and Applications, Setúbal, vol. 2, pp. 116–121.